SISSA

Optical links for detector instrumentation: on-detector multi-wavelength silicon photonic transmitters

To cite this article: D. Karnick *et al* 2017 *JINST* **12** C03078

View the article online for updates and enhancements.

Related content

- System-level testing of the Versatile Link components
  C Soós, S Détraz, L Olanterä et al.

- Development of the ABCStar front-end chip for the ATLAS silicon strip upgrade
  W. Lu, F. Anghinolfi, L. Cheng et al.

- Versatile transceiver production and quality assurance
  L. Olantera, S. Detraz, C. Sigaud et al.

Optical links for detector instrumentation: on-detector multi-wavelength silicon photonic transmitters

D. Karnick,[1] **P. Skwierawski, M. Schneider, L. Eisenblätter and M. Weber**

Karlsruhe Institute of Technology, Institute for Data Processing and Electronics,
Hermann-von-Helmholtz-Platz 1, 76344 Eggenstein-Leopoldshafen, Germany

E-mail: djorn.karnick@kit.edu

ABSTRACT: We report on our recent progress in developing an optical transmission system based on wavelength division multiplexing (WDM) to enhance the read-out data rate of future particle detectors. The design and experimental results of the prototype of a monolithically integrated multi-wavelength transmitter are presented as well as temperature studies of electro-optic modulators. Furthermore, we show the successful permanent coupling of optical fibers to photonic chips, which is an essential step towards packaging of the opto-electronic components.

KEYWORDS: Optical detector readout concepts; Front-end electronics for detector readout

---

[1]Corresponding author.

Contents

1 Introduction

Future experiments in high-energy physics (HEP), nuclear physics, photon science or materials research show an ever-increasing number of detector channels [1]. Volume and mass of the cables and energy consumption of the front-end electronics should be low to minimize multiple scattering. An optical data transmission system offers a large data transmission rate and satisfies the requirements on low power, volume and mass [2].

In state-of-the art detector systems, directly modulated laser diodes are used as optical transmitters operating at data rates of up to 10 Gbit/s. Individual optical fibers connect each transmitter inside the detector volume to a receiver in the periphery [3].

Recently, we proposed an optical transmission system based on wavelength division multiplexing (WDM) [4], a technique quite common in optical long-haul networks. A simplified schematic is depicted in figure 1a). An off-detector laser source generates stabilized optical carriers at wavelengths λ_i, which are multiplexed and conveyed over a single optical fiber to a multi-wavelength transmitter module (Multi-λ Tx) inside the detector volume. The transmitter is sketched in figure 1b). All components are monolithically integrated on a photonic integrated circuit (PIC). An optical demultiplexer (DEMUX) separates the incident carriers λ_i. Each is forwarded to a Mach-Zehnder modulator (MZM), which encodes electrical data from the front-end electronics. The data-carrying optical channels are re-multiplexed and guided back to the data center or counting room on a single optical fiber. The system is fully transparent to the front-end and data-acquisition (DAQ) electronics. It increases the data read-out capacity significantly while reducing the number of individual fibers connecting the detector with the DAQ units.

In this paper, we present our recent progress in the development of an optical transmission system for detector data read-out. We show the design and experimental results of a next-generation integrated optical four-channel transmitter with silicon-organic hybrid (SOH) modulators [5] and planar concave grating (PCG) (de-)multiplexers [6, 7]. The SOH-platform allows for compact and

power-efficient modulators. It is an emerging technology, which is not optimized for the stringent requirements of particle physics. Therefore, we also investigate the suitability of depletion-type pn-modulators [8]. We show the result of a study on the influence of ambient temperature on their modulation characteristics. Finally, we discuss our activities in packaging the transmitter PIC. Two methods of coupling standard single-mode fibers (SMF) permanently to an opto-electronic component are presented and evaluated.

2   System design and on-detector transmitter

Our transmitter consists of monolithically integrated MZM and optical filters for (de-)multiplexing optical carriers. Two phase shifter technologies are considered for the MZM design. For one, carrier depletion-type pn-modulators, where the active region of a pn-junction integrated in the photonic waveguide is depleted by a reverse bias voltage. Due to the plasma-dispersion effect, free charge carriers govern the refractive index and hence the optical field's propagation velocity. For short-reach interconnects, a more recent approach is the silicon-organic hybrid (SOH) technology. Phase modulation of the optical field is achieved by interacting with an electro-optically active organic material inside a slot waveguide.

PCG-(de-)multiplexers split or merge optical carriers by means of diffraction. An incident optical field propagates through a two dimensional free-space region, where it diverges. It is reflected at a concave grating and refocused on a series of output ports depending on its wavelength.
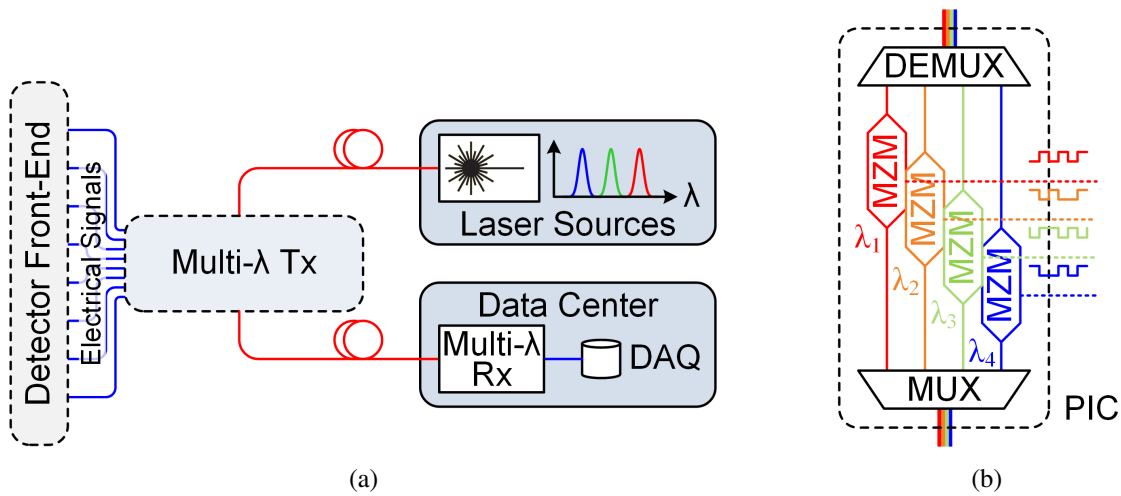

Figure 1. Schematic of the envisioned optical data transmission for HEP detectors. An off-detector laser source generates multiple optical carriers on which the on-detector transmitter encodes electrical signals from the detector front-end (a). Detailed schematic of the integrated four-channel transmitter (b).

Figure 2a) shows a photograph of a photonic chip with 3 transmitter units. Each unit incorporates four modulators, a demultiplexer and a multiplexer. The design has been fabricated at *Institut für Mikroelektronik* Stuttgart, Germany (IMS-CHIPS) [9]. The total dimension of the chip is $10 \times 10 \, \text{mm}^2$. Several other modulators, PCG-multiplexers and test structures are included, too.

The inset in figure 2a) shows the mask layout of one transmitter unit. In the upper area, four SOH-MZM with a slot width of 160 nm are aligned in parallel. The length of the phase

shifters is 1000 µm. Including feed line and contacting pads, the MZM are 3.4 mm long. Each is connected to one port of the (de-)multiplexer located in the lower area. The optical input and output are implemented by grating couplers with a bandwidth (FWHM) of 40 nm to attach optical fibers. In addition, supplementary grating couplers provide direct access to the modulators for characterization measurements.

Figure 2b) shows the transmission spectrum of the entire transmitter unit. It is obtained by sweeping the wavelength of a tunable laser source (Agilent 81689A) and measuring the mean optical power transmitted through the unit with an optical power head and interface (Agilent 81623B and 81618A). The modulators are biased for maximum transmission. Four channels with a bandwidth of 2 nm FWHM separated by 7 nm can be distinguished. The transmission window of the channel centered at 1522 nm is not shown completely because it is beyond the tuning range of our laser. The total loss of the three visible channels is 20 dB or less. The suppression of adjacent channels is larger than 25 dB.
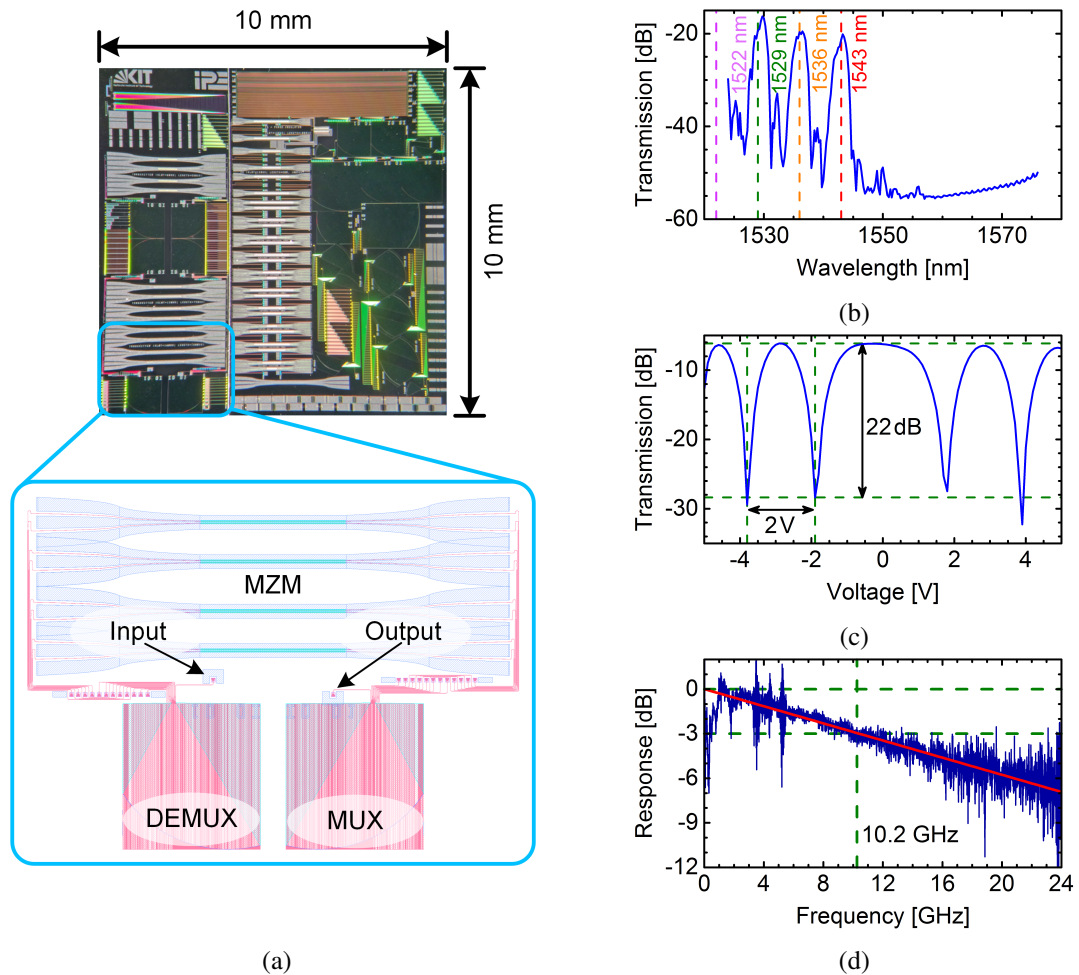

Figure 2. Microscope image of a photonic chip with three transmitter units one underneath the other on the left-hand side and an excerpt of the mask layout for a detailed view (a). Transmission spectrum of the entire transmitter unit (b). Steady-state transmission characteristic (c) and electrical-optical-electrical (EOE) response (d) of one of the integrated MZM.

Figure 2c) shows the steady-state transmission characteristic of one of the MZM in the voltage range of −5 V to 5 V. A commercially available organic material is used. At −3 V bias voltage, an extinction ratio of 22 dB is obtained with a corresponding voltage-length product $V_\pi L$ of 1 Vmm. By using novel organic materials, this value may even be further reduced [10]. The electrical-optical-electrical (EOE) response is shown in figure 2d). This result is obtained by using a vector network analyzer (Rohde&Schwarz ZVA24), a cw-laser source and a photodetector (New Focus 1014). The dark blue curve represents the measured EOE response, while the solid red and the dashed green lines serve to guide the eye. The result shows a 3 dB bandwidth of 10.2 GHz. A higher bandwidth could be achieved by increasing the conductivity of the feeders. However, the transmitter is suitable for a total data rate of 4×10 Gbit/s and beyond while requiring only a voltage swing less than 1 V.

3   Temperature studies of Mach-Zehnder modulators

The performance of silicon photonic devices significantly depends on ambient temperature. A transmitter in a HEP detector may have to operate reliably at temperatures as low as −10°C [11]. Below we investigate the temperature sensitivity of MZI-based electro-optic modulators. Note that the phase shifters are depletion-type pn-modulators.

In figure 3a), a schematic of the measurement setup is depicted. The device under test (DUT) is characterized using a specially designed sample holder with water-cooled, stacked Peltier elements. To prevent short circuits due to condensing humidity, the sample holder is flooded with dielectric fluid (3M Novec 7500). The DUT is optically probed with cleaved standard single-mode fibers. The temperature is monitored by measuring the resistance of a Pt100 temperature sensor. The results are obtained by sweeping the wavelength of the tunable laser source and measuring the mean optical power with an optical power head and interface as described in section 2. The polarization of the incident optical field is adjusted manually with a polarization controller. Bias voltage for the modulators is provided by a source meter unit (Keithley 2400) and applied with an electrical probe.

The steady-state modulation efficiency is analyzed by measuring the transmission spectra of an antisymmetric MZM at different bias voltages. Transmission minima are shifting by an interval $\Delta\lambda_i$ when a voltage V_i is applied. The modulation efficiency is given by the relative phase shift which equals the ratio of $\Delta\lambda_i$ and the free spectral range of the interferometer [12].

Figure 3b) shows the result of the temperature characterization of a 3 mm long MZM. It consists of depletion-type pn-modulators from a commercially available design provided by the *OpSIS* project [4, 13]. In figure 3a), the relative phase shift as a function of the bias voltage is shown for different operating temperatures in the range from −28°C to 57°C. A phase offset of less than $0.05\,\mathrm{K}^{-1}$ is observed upon temperature variation, which occurs due to the thermo-optic effect [14]. The modulation characteristic remains unchanged. Hence, in practice an adjustment of the modulator bias voltage easily compensates for the shift of the operating point without affecting the signal quality.
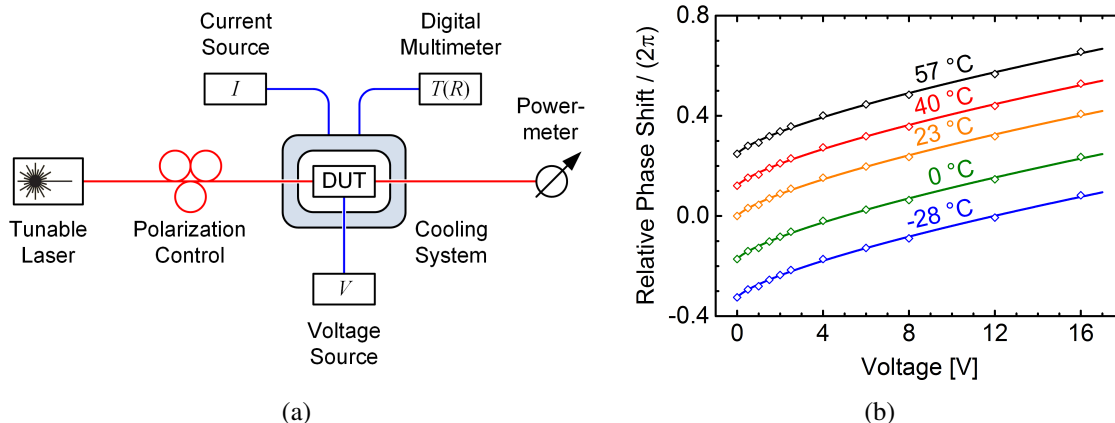
Figure 3. Sketch of the temperature characterization setup (a). Steady-state modulation efficiency represented by the relative phase shift as a function of bias voltage at different temperatures. All values are normalized to the phase at 0 V and room temperature (b). The systematic error in the order of less than 0.1 is suppressed for clarity.

4 Fiber-to-chip coupling for packaging of opto-electronic components

In order to construct a functional module from the aforementioned opto-electronic devices, packaging and in particular a permanent fiber-to-chip coupling is required. Due to the mismatch of the refractive indices and mode field diameters of SMF and silicon photonic waveguides, a mode converter is required for the coupling. A convenient way is to make use of grating couplers [15]. Then the optical mode is coupled from the fiber to the waveguide and vice versa at a small angle with respect to the chip surface normal.

4.1 Development of coupling process

Figure 4a) shows a photograph of a self-designed preliminary surface coupling design. A PIC is mounted on a standard glass substrate and fixed with heat-curing epoxy. Two cleaved SMF are mounted on aluminum sockets which are milled so as to provide the appropriate coupling angle for the grating couplers. The sockets are aligned by stepper motors and piezo-driven handling stages and fixed with acrylate-based UV-curing adhesive. The inset in figure 4a) shows a close-up of the fiber facets aligned towards the PIC surface. At the size of $20 \times 10 \times 20 \, \text{mm}^3$ (l × w × h) the structure is large compared to the photonic component. Although the dimensions could be further reduced, the minimum height is governed by the bending radius of the optical fibers. However, the main purpose of this arrangement is to investigate the process handling and adhesive characteristics.

To assess the long-term stability of the arrangement, the total coupling efficiency in non-stabilized environment is observed. Figure 4b) shows the coupling efficiency normalized to the highest measured value as a function of the elapsed time since assembly. Each data point represents the mean coupling efficiency measured over several hours. Sources of uncertainty are re-plugging of fiber connectors and polarization adjustment, which explains the scattering of the data points. Apart from the uncertainties, no significant loss is recognized over more than six months. Hence, the assembly is considered to be long-term stable.
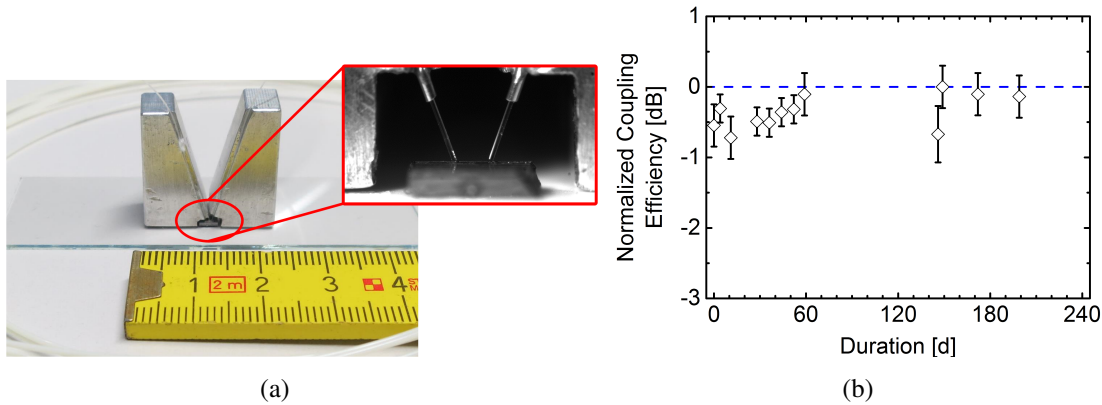
Figure 4. Setup and result of a preliminary fiber-to-chip coupling arrangement. Photograph of the assembly, with a close-up of the fibers aligned towards the grating couplers of a PIC (a). Long-term coupling efficiency normalized to the highest coupling value (b). The total insertion loss of the PIC test structure is 16 dB.

In order to assess the influence of environmental conditions on the assembly, studies of the coupling stability with respect to ambient temperature and humidity in a climate testing cabinet (Weiss Type WK3-340/40) are performed. Humidity is a critical parameter, since acrylate-based adhesives tend to behave hygroscopically. That typically involves a change in volume of the adhesive layer which may result in increased coupling loss.

Figure 5a) shows the coupling efficiency as a function of the relative humidity in the range of 30%, which is close to the humidity during assembly, to 80%. The humidity is changed with a rate of 2% per hour which gives the assembly ample time to adapt. Even at 80% relative humidity, the coupling loss is only 0.2 dB. Furthermore, the change in coupling efficiency is totally reversible.

In figure 5b), the dependency of the coupling efficiency on ambient temperature from 20°C to 80°C is shown. After changing the temperature, the coupling efficiency is measured only after it has stabilized. A maximum loss of 16 dB at 80°C is recognized. This is attributed to the thermal expansion of the aluminum sockets leading to a severe misalignment of the fibers. However, the degradation is also reversible once the initial temperature is restored.

4.2 Size reduction

The drawback of the coupling arrangement presented in section 4.1 is the large dimension and in particular the height of the sockets. Therefore, a planar arrangement for a horizontal fiber-to-chip coupling is constructed and characterized. The scheme is outlined in figure 6a). The facet of a SMF is polished at an angle smaller than 45°. By means of total internal reflection, the optical field is coupled from the fiber to the grating coupler and vice versa radially with respect to the fiber axis. The concept is quite well-known for the coupling of photodetectors and laser diodes [16, 17], but has only recently been introduced for the surface coupling of silicon photonic waveguides [18]. We adapt this concept and develop an easy-to-use fiber-to-chip coupling process suitable even for component characterization purposes.

A photograph of the planar fiber-to-chip coupling assembly is presented in figure 6b). Two angle-polished optical fibers are attached to grating couplers on the photonic chip. They are mounted on standard v-groove chips, which can be positioned with appropriate precision alignment
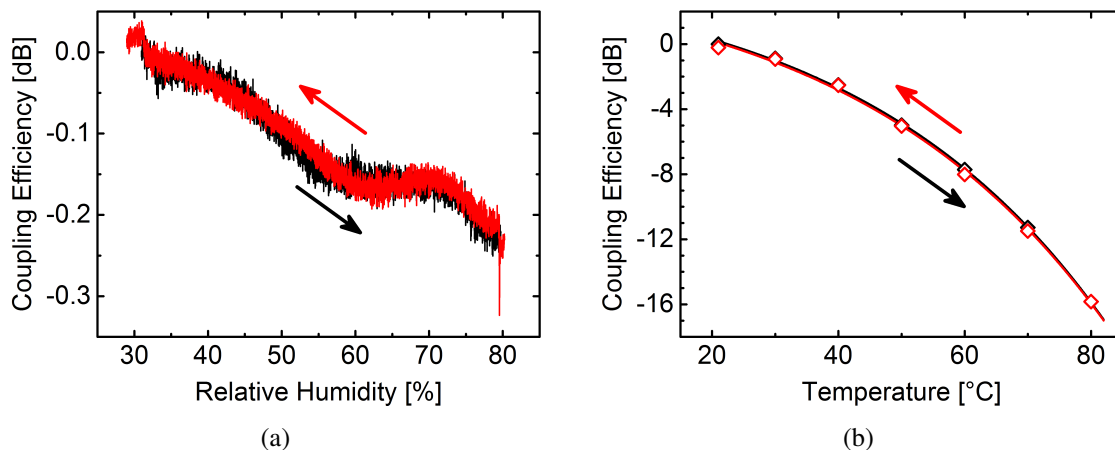
Figure 5. Relative coupling efficiency of the preliminary fiber-to-chip coupling arrangement as a function of ambient humidity (a) and temperature (b). The black curves represent the measured efficiency during the continuous increase of humidity or temperature, respectively, while the red curve is obtained during the decrease.
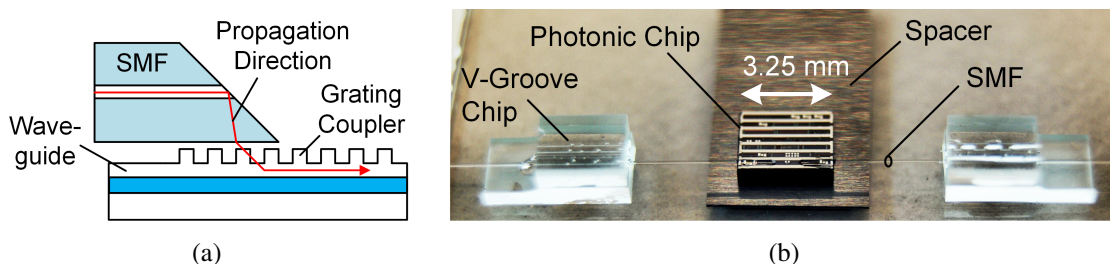

Figure 6. Functional principle (a) and a photograph (b) of a fiber-to-chip coupling arrangement with angle-polished fibers to provide for a planar arrangement.

equipment. Similar to the preliminary setup in section 4.1, fibers and sockets are fixed with UV-curing adhesive. The photonic chip is elevated by a spacer to minimize the gap between the fibers and the chip surface. All components are mounted on a glass substrate. Mechanical stability is ensured by also bonding the fibers to the chip surface. In comparison to the assembly in figure 4a), the spatial requirements are reduced substantially. The dimensions now are $20 \times 5 \times 2\,\text{mm}^3$ (l × w × h), with the potential for further reduction. Especially the fiber sockets can easily be placed closer to the photonic chip.

The result of the investigation of the long-term coupling efficiency in non-stabilized environment is depicted in figure 7a). Measurement uncertainties cause scattering of the data points. No significant loss is observed over more than 3 months. Finally, the dependency of the coupling efficiency on ambient temperature is investigated. Figure 7b) shows the coupling efficiency as a function of ambient temperature in the range of 20°C to 80°C. Optimum is achieved at 20°C. Apparently, the coupling efficiency is only weakly dependent. The loss at 80°C is smaller than 2 dB, which is a great advance compared to the preliminary structure in figure 4a). As expected, smaller dimensions and the absence of metal significantly reduce the influence of ambient temperature on the coupling efficiency.
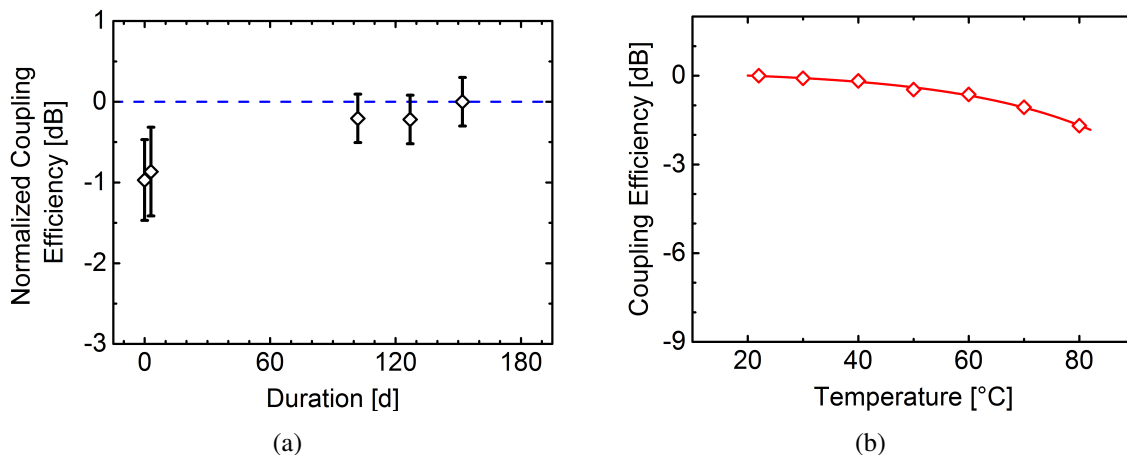
Figure 7. Measurement results of the planar fiber-to-chip coupling arrangement. Long-term coupling efficiency normalized to the highest coupling value (a). Relative coupling efficiency as a function of the ambient temperature (b). The total insertion loss of the PIC test structure is 13 dB.

5 Conclusion

Energy-efficient high-speed data read-out is an essential aspect in the development of any future detector system. A WDM-based optical transmission system significantly increases the read-out bandwidth while the number of optical fibers can be reduced. We have presented and discussed recent progress in the development of a multi-Gbit/s optical link. An integrated on-detector four-channel transmitter based on SOH-modulators offers a per-fiber data rate of at least 40 Gbit/s with a modulator driver voltage swing as low as 1 V. The technology allows for efficient modulators, but is still emerging and not yet optimized for the environment of particle physics detectors. Varying the temperature from $-28°C$ to $57°C$ does not change the modulation efficiency of a depletion-type Mach-Zehnder modulator. The result is a constant phase offset of $0.05\,K^{-1}$ only, which can be compensated by a shift of the operating point. Finally, with a long-term stable, low-profile fiber-to-chip coupling arrangement, we accomplished an essential step towards packaging the optical transmitter. A planar arrangement is achieved with angle-polished standard single-mode fibers, which provide for total internal reflection of the optical field.

References

[1] S. Papadopoulos et al., *A network architecture for bidirectional data transfer in high-energy physics experiments using electroabsorption modulators*, in *16th European Conference on Networks and Optical Communications (NOC)*, July 2011, p. 68.

[2] C.D. Via et al., *Lightwave analogue links for LHC detector front-ends*, *Nucl. Instr. Meth.* **A 344 (1994) 199**.

[3] F. Vasey, *Optical links for LHC: experience from the CMS project and future prospects*, in *10th Workshop on Electronics for LHC and Future Experiments*, September 2004, p. 31.

[4] P. Skwierawski et al., *A silicon photonic wavelength division multiplex system for high-speed data transmission in detector instrumentation*, 2016 *JINST* **11** C01045.

[5] J. Leuthold et al., *Silicon-organic hybrid electro-optical devices*, *IEEE J. Sel. Top. Quant.* **19** (2013) 114.

[6] D. Chowdhury, *Design of low-loss and polarization-insensitive reflection grating-based planar demultiplexers*, *IEEE J. Sel. Top. Quant.* **6** (2000) 233.

[7] R.J. Lycett et al., *Perfect chirped echelle grating wavelength multiplexor: Design and optimization*, *IEEE Photonics J.* **5** (2013) 2400123.

[8] G.T. Reed, F.Y. Gardes, G. Mashanovich and D.J. Thomson, *Silicon optical modulators*, *Nat. Photonics* **4** (2010) 518.

[9] M. Kaschel et al., *Echelle grating for silicon photonics applications: integration of electron beam lithography in the process flow and first results*, *Proc. SPIE* **9891** (2016) 98911V.

[10] S. Koeber et al., *Femtojoule electro-optic modulation using a silicon-organic hybrid device*, *Light Sci. Appl.* **4** (2015) e255.

[11] J. Troska et al., *Optical readout and control systems for the CMS tracker*, in *IEEE Nucl. Sci. Conf. R.* **1** (2002) 233.

[12] A. Liu et al., *High-speed optical modulation based on carrier depletion in a silicon waveguide*, *Opt. Express* **15** (2007) 660.

[13] T. Baehr-Jones et al., *A 25 Gb/s silicon photonics platform* (2012) `arXiv:1203.0767`.

[14] B. Guha et al., *Minimizing temperature sensitivity of silicon Mach-Zehnder interferometers*, *Opt. Express* **18** (2010) 1879.

[15] D. Taillaert et al., *Grating couplers for coupling between optical fibers and nanophotonic waveguides*, *Jpn. J. Appl. Phys.* **45** (2006) 6071.

[16] I. Ladany, *Laser to single-mode fiber coupling in the laboratory*, *Appl. Opt.* **32** (1993) 3233.

[17] Y. Oikawa et al., *Packaging technology for a 10-Gb/s photoreceiver module*, *J. Lightwave Technol.* **12** (1994) 343.

[18] B. Snyder and P. O'Brien, *Packaging process for grating-coupled silicon photonic waveguides using angle-polished fibers*, *IEEE Trans. Compon. Packag. Manuf. Technol.* **3** (2013) 954.